



Striations in YIG fibers grown by the laser-heated pedestal method

Han-Jin Lim^a, Robert C. DeMattei^b, Robert S. Feigelson^{b*}, Kent Rochford^c

^a*Samsung Electronics, South Korea*

^b*Center for Materials Research, Stanford University, 111 McCullough Buildings, Stanford, CA 94305-4045, USA*

^c*Optoelectronics Division, NIST, Boulder, CO 80303-3328, USA*

Received 16 November 1998; accepted 24 November 1999

Communicated by P.A. Morris Hotsenpiller

Abstract

Yttrium iron garnet (YIG) single-crystal fibers of nominal composition $Y_3Fe_5O_{12}$ were grown by the laser-heated pedestal growth technique, a miniaturized float-zone process. YIG fibers in diameters ranging from 100 to 740 μm were grown at various rates and conditions, and analyzed by X-ray diffraction, electron microprobe, IR-VIS spectroscopy, and light scattering tomography. Infrared transparent YIG fibers were grown at rates below 10 mm/h in air. The transparency of the fibers was more dependent on the growth rate than on the stability of the molten zone. Some striations and surface ridges containing a Fe-rich composition were observed at all growth rates. Light scattering tomography studies revealed the presence of inclusions in some YIG fibers. Their size, density, composition and distribution depended on the growth conditions and molten zone stability. At growth rates below 10 mm/h, these defects and also the iron-oxide inclusions, which act as IR scattering centers, were significantly reduced. Q 2000 Elsevier Science B.V. All rights reserved.

Keywords: YIG; Float-zone method; Traveling solvent zone method; Solution growth; Laser-heated pedestal growth; Light scattering - tomography

1. Introduction

$Y_3Fe_5O_{12}$ (YIG) is one of a well-known family of ferrimagnetic materials. It was first synthesized in the mid 1950s [1-3]. Since then this material has been widely studied because of its excellent microwave properties including relatively low magnetization, extremely narrow line width and low dielectric loss behavior [4,5]. These properties make it suitable for microwave devices such as circulators, isolators, and phase shifters. YIG also has unique magneto-optical properties in the near infrared (1-5 μm) [6,7], and is also useful as an infrared isolator, optical switch, spatial light modulator, and in sensor applications.

Polycrystalline YIG can be prepared by conventional ceramic processing methodologies [8-10]. The best density reported for a YIG ceramic was 99% of the theoretical which was obtained by hot pressing

*Corresponding author. Fax: +1-650-723-3752
E-mail address: feigel@ee.stanford.edu (R.S. Feigelson).

techniques [10]. For most applications single crystals have better magneto-optic properties than polycrystalline material [5-7] so there has been considerable effort in this area. YIG is an incongruently melting compound as can be seen from the phase diagram given in Fig. 1 [11,12]. This makes crystal growth by many commonly used melt growth methods difficult. Single crystals of bulk YIG have been grown by the flux [13-16] and traveling solvent float-zone (TSFZ) methods [17-21]. The float-zone process [22] is one of the best methods for growing uniform single crystals of this type of compound and the laser-heated pedestal growth (LHPG) technique [23] used in this fiber growth study is basically a miniaturized float-zone process. The conclusions reached in Refs. [18-20] on the float-zone growth of YIG were, therefore, directly relevant to this research effort.

The ideal transparency of YIG in the infrared region for general multipath reflections is about 75% [24]. However, YIG single crystals grown by the TSFZ method have not always shown good transparency [25]. The poor transparency of YIG crystals has been ascribed to a broad optical absorption resulting from a lack of stoichiometry in the garnet. This nonstoichiometry leads to a fluctuation in the charge of the matrix iron ions from Fe^{3+} to Fe^{2+} or Fe^{4+} [26]. Since transparency is of critical importance in magneto-optic applications, a variety of techniques, including precision doping and/or heat treatment in either oxygen or reducing atmospheres have been applied to both float zone and flux grown YIG in order to maintain the iron in its Fe³⁺ oxidation state [24,26].

In addition to matrix absorption, both inclusions and striations can strongly affect the optical quality of float-zone crystals. In this report, the main focus is on the formation of striations during laser-heated fiber growth and the factors which cause them.

For the preparation of 100-400 gm single-crystal fibers, LHPG was chosen because laser heating permits the formation of small molten zones. This growth method is containerless and therefore contamination and stress problems are reduced. Very high temperatures can be achieved rapidly, as well as very steep temperature gradients. The steeper temperature gradients and small diameters permit faster growth rates when compared to bulk crystal growth.

2. Experimental Procedure

Starting with a YIG seed and source rod, steady-state growth of YIG can be achieved from an Fe_2O_3 -rich solution whose composition gives a liquid phase below the peritectic decomposition temperature (Fig. 1). While the growth rates will be lower than those from a pure melt, due to partitioning effects, the high-temperature gradients in the LHPG system allow much greater rates than those encountered in normal flux growth.

The growth experiments described below were concerned with preparation of pure YIG fibers using a dense YIG polycrystalline source.

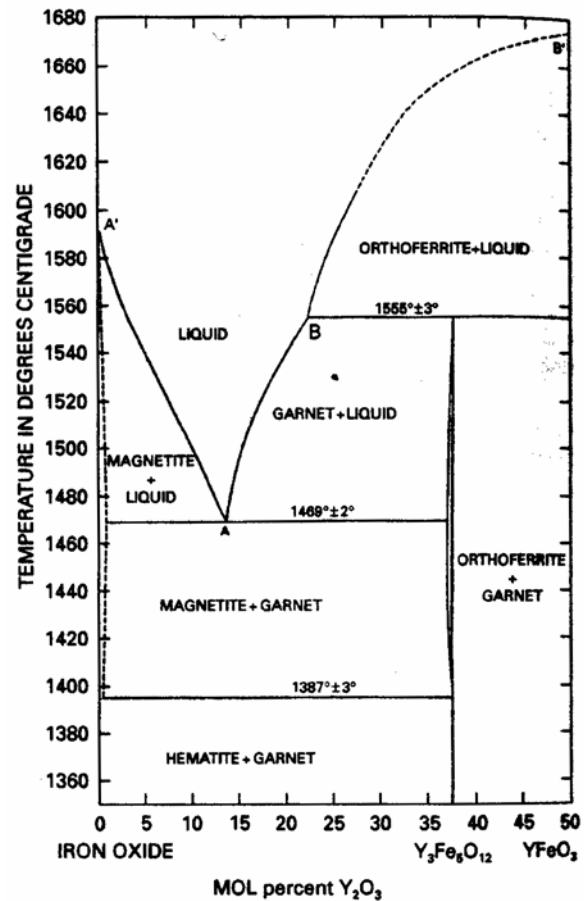


Fig. 1 Fe_2O_3 - $YFeO_3$ section of the iron oxide-yttrium oxide phase diagram in air [11].

2.1. Fabrication of YIG source rod

Hot pressed polycrystalline YIG bulk material was used in this study. It was prepared in our laboratory a number of years ago. It had a density 92% of theoretical, and was cut into bars approximately 1 mm x 1 mm square and 25 mm long. Some of these were microground into 300 gm diameter rods. Dense source material is helpful in reducing molten zone instabilities caused by partially unreacted or porous source material. Singlecrystal YIG fibers or platinum wires were used as a seed material.

2.2. YIG fiber growth

Fibers were grown in lengths up to 40 mm and with diameters ranging from 100-740 gm (uniform diameters could be maintained in the range of 350-500 gm). Growth rates were initially varied between 8 and 60 mm/h. Fibers were grown in air or oxygen atmosphere.

The fiber growth apparatus is described in Ref. [23]. The beam from a 50 W CO₂ laser, operating at 10.6 μm, is expanded and focused into an annular beam at the end of a rod of the material to be grown into a fiber. The laser and growth station are mounted on a vibration-damped table and the growing crystal and molten zone are observed through a binocular microscope with variable magnification to 70 x. The amount of power necessary to melt a material is a function of the source rod diameter and the emissivity of the material. Oxide materials absorb 10.6 μm radiation very effectively. A nominal 50 W CO₂ laser provides sufficient power to melt a YIG specimen 2 mm or smaller in diameter, as shown in the plot of Fig. 2. However, when the source rod is less than 500 gm, the power required to form the molten zone is so small that it is difficult to maintain laser, and hence zone stability. The use of an attenuator, however, allows the laser to operate in a stable mode at mid-power levels, even when less than 10 W is required for melting. The angle of the beam, beam diameter and shape, and laser stability are important factors in determining the shape and stability of the molten zone and the quality of the crystals produced.

In the pedestal growth method, the fiber diameter is typically between 1/2 to 1/3 the diameter of the source rod and so the ratio of fiber-to-source rod pull rates has to be adjusted accordingly. The concept of LHPG is shown schematically in Fig. 3.

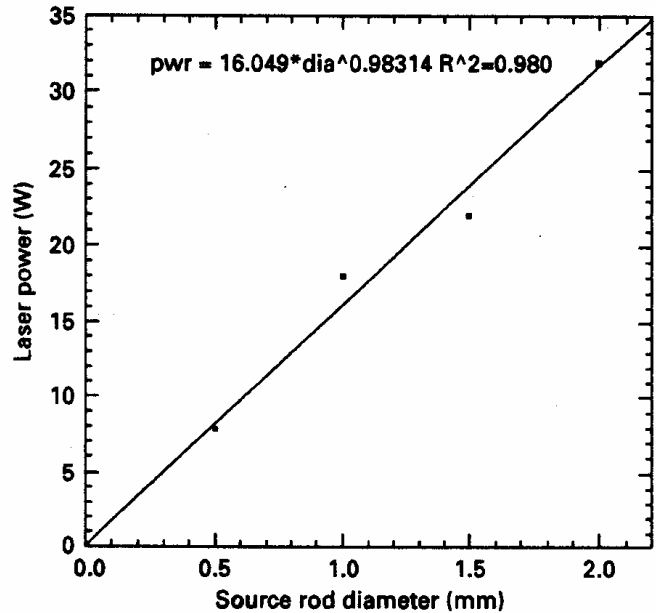


Fig. 2 Laser power versus YIG source rod diameter.

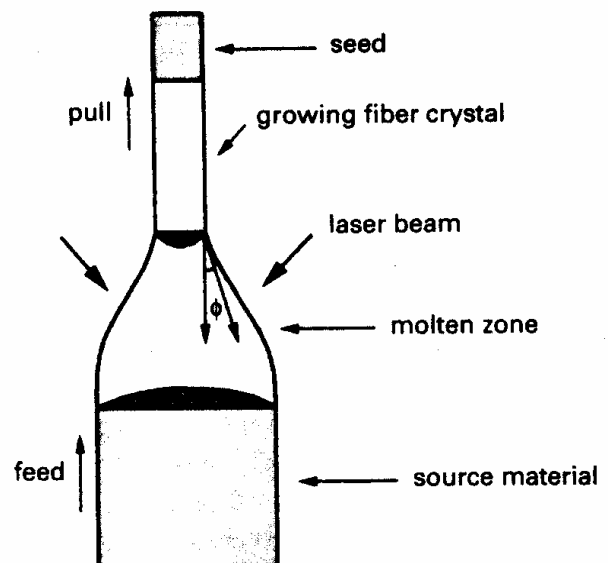


Fig. 3 Schematic diagram of fiber growth process.

2.3. Characterization

The crystalline quality of the source material and YIG fibers was determined using a four-circle X-ray diffractometer. The fiber surface morphology was analyzed using scanning electron microscopy (SEM). The composition of the fibers, molten zones and large second phase inclusions were determined by electron microprobe analysis (EPMA) using Y_2O_3 and Fe_2O_3 as standards. Infrared transparency was examined by both IR spectroscopy and a CCD camera. Finally, high-resolution light scattering tomography (LST) was used to image very small defects such as inclusions, dislocation and twin boundaries. The light scattering tomography apparatus consists of a 33 mW Nd : YAG (1.064 μm) laser focused to a narrow beam inside the crystal, a three-axis translation stage for scanning, and a microscope and CCD camera interfaced with a computer for recording images. Microscope were changed from low power for imaging large fields to high power for imaging at high resolution. A horizontal slice of the specimen in the xz -plane of the system was obtained by scanning the crystal along the x -direction of the system and forming a composite image from the narrow strips that are successively illuminated by the laser beam.

3. Results and Discussion

3.1. YIG fiber growth

Twenty-one YIG fibers were grown by the LHPG method. Information on the type of seed used, the composition, size and shape of the source material, the growth conditions, and the fiber dimensions are given in Table 1. Table 1 also includes the ratio of seed-to-source rod diameter (d/D) used in each experiment.

Samples 1-5 in Table I focused on the variation of growth rates, which ranged from 10 to 60 mm/h. The polycrystalline YIG source rods had either round or square cross sectional shapes in sizes ranging from 0.5 to 1 mm. The reduction ratio (d/D) was about 1/2.

Table 1 Summary of YIG fiber growth by the laser-heated pedestal growth method

Sample No.	YIG ID	Seed	Source Type	Source		d/D^a	Growth Rate (mm/h)	Molten Zone Temp (°C)	Atm	Length (mm)	Diameter (μm)
				Shape	Size (mm)						
1	YIG-1-1	Single Fiber	Pressed	Round	~0.5	1/2	60		O ₂	~40	~250
2	YIG-1-2	Fiber	Pressed	Round	~1	1/2	40		Air	~35	~600
3	YIG-1-3	Fiber	Pressed	Round	~0.5	1/2	30		O ₂	~15	~250
4	YIG-1-4	Fiber	Pressed	Square	1 x 1	1/2	~20		O ₂	~15	~500
5	YIG-2	Fiber	Pressed	Square	1 x 1	1/2	10-12		O ₂	2 x 6	~500
6	YIG-5-1	Fiber	Pressed	Square	1 x 1	1/2	12	1650-1690	Air	~500	~25
7	YIG-5-2	Fiber	Pressed	Square	1 x 1	1/3	12	1620-1675	Air	~25	~330
8	YIG-6-1	Fiber	YIG-5-2 (#7)	Round	~0.33	1/3	12		Air	23	~120
9	YIG-7	Fiber	YIG-5-2 (#6)	Round	~0.50	<1/3	~12	1680	Air	15	~100
10	YIG-8-1	YIG-1(#1)	Pressed	Square	1 x 1	1/3	~12	1660-1690	Air	35	~330
11	YIG-8-2	Fiber	Pressed	Square	1 x 1	~1/2	12	1660	Air	15	~500
12	YIG-8-3	YIG-7 (#8)	Pressed	Square	1 x 1	<1/2	12	1635	Air	30	~400
13	YIG-9-1	YIG-7	Pressed	Round	0.325	1/2	~10		Air	15	~100
14	YIG-9-2	YIG-7	Pressed	Round	0.325	1/2	~10		Air	10	~150
15	YIG-10-1	Fiber	Pressed	Round	0.325	~1	<10		Air	5	~300
16	YIG-11	Pt. Wire	Pressed	Square	1 x 1	1/3	10	1620-40	Air	7	~330
17	YIG-12-1	Fiber	Pressed	Round	0.325	1/2	10	1580-1640	Air	5	~150
18	YIG-12-2	Fiber	Pressed	Round	0.325	1/2	10	1650	Air	5	~150
19	YIG-13	Fiber	Pressed	Square	1 x 1	~3/5	<10	1590-1640	Air	20	~600
20	YIG-14	Fiber	Pressed	Square	1 x 1	~2/3	<10	1600-1650	O ₂	~15	~740
21	YIG-14-2	Pressed	Pressed	Square	0.85 x 0.95	~1/2-2/3	<10	1570 (air), 1620 (O ₂)	Air/O ₂	~25	~730, 480

^aReduction ration (d/D): diameter of fiber/diameter of source rod

Samples 7-21 were slow-growth experiments (less than 12 mm/h) and were designed to maintain the compositional uniformity of YIG fibers. With the exception of samples 8 and 9, which used sections of previously grown fibers as source material, samples 6-12, 16, and 19-21 were grown from source rods with a square cross section. This in itself can lead to some inhomogeneities in the heating of the source rod, and also to melt instability.

Fibers 13, 14, 15, 17, and 18 were grown using source rods with a circular cross section obtained by centerless grinding to 0.325 mm diameter. YIG fibers with less than 150 μm diameter were prepared from these source rods for magneto-optical measurements.

A YIG fiber of fairly uniform diameter (10 in Table 1) was grown to a length of 11 mm. A scanning electron microscope image of this fiber (Fig. 4) verifies the constant diameter.

3.2. Infrared microscopic study

Bands and inclusions in YIG fibers could be seen with an IR microscope (wavelength in the range of 0.7-1.1 μm). The best results were obtained by grinding flats on opposite sides of the fiber. A test section taken from fiber 10 was transparent as viewed through the IR microscope normal to the fiber axis (the short dimension). Fig. 5 shows the image viewed through the IR transmission microscope normal to the polished fiber axis. A scratch in the glass plate below the fiber can clearly be seen.

While the use of the IR microscope allowed us to survey the optical transparency of the fiber rather quickly, the grinding process is tedious and modifies the shape of the fiber so that it is not very satisfactory for follow-up device measurements. To eliminate the need for grinding and polishing these fibers, an index matching fluid ($I = 1.52$) was used to observe as grown fibers by IR microscopy or with a CCD camera. Although this fluid does not closely match the index of YIG, it is better than air. With this method, impurity striations, bands, or inclusions could be observed in the fiber without polishing it.

The results of IR studies of YIG fibers are shown in Table 2. Most of YIG fibers contain internal impurity bands, or inclusions. At fast growth rates, these striations are dominant. When the growth rate was decreased, these bands were significantly reduced but not completely eliminated.

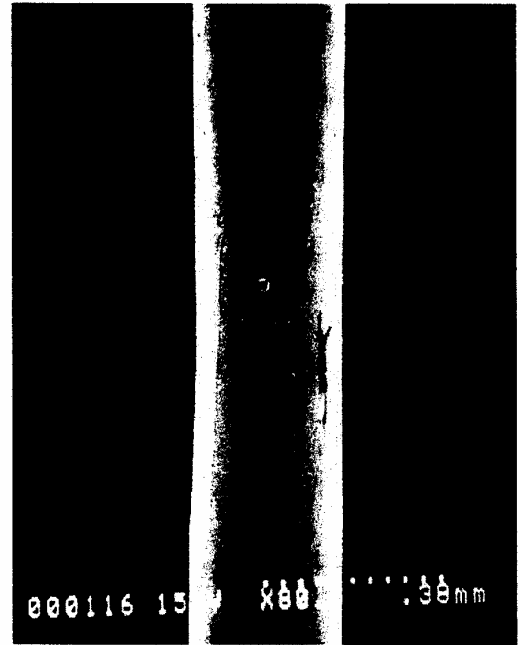


Fig. 4 SEM image of fiber sample No. 10 at 80x.

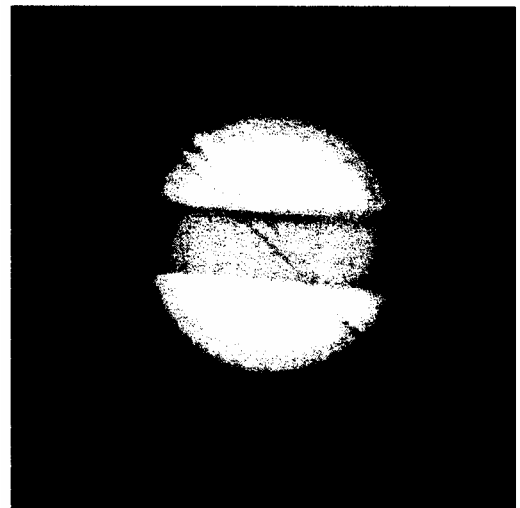


Figure 5 Infrared microscope image of fiber sample No. 10.

Table 2 Observation of pure YIG fibers immersed in index matching fluid ($n = 1.52$) by IR microscope

Sample No.	Transparency
1-4	Not very transparent (black inclusions, striations)
5	Very poor transparency
6	Transparent with black inclusions
9	Not very transparent (black inclusions, striations)
10	Transparent with striations or inclusions
11	Very poor transparency
12	Central part (~10 mm): transparent with a few striations
14	Very transparent in some 2-3 mm section along axis
16 (7 mm long)	Transparent with striations, inclusions
16 (5 mm long)	Almost completely opaque
18	Very transparent in some sections (>5 mm) along axis
19	Transparent except both ends (~10 mm)
20	Short transparent region, most of fiber opaque
21	Transparent (the part grown in air), not transparent (the part grown in oxygen)

Some of the 150 μ m diameter fibers (such as 14 and 18) were very transparent at 1.1 μ m in some 3-5 mm sections along the fiber axis. The iron oxide tipped sample, fiber 19, had a well-controlled fiber diameter (~600 μ m) for 20 mm. Fig. 6 shows IR transmission images of fiber 19. Two sides of the fiber were polished along its length in order to observe its transparency. This fiber was immersed in an index matching fluid, which allows some light to pass through the fiber. The unpolished curved outer edges appear dark. Striations, caused either by impurities or stoichiometric variations, can clearly be seen even though this fiber was grown at a growth rate similar to or slightly lower than fibers 14 and 18. The larger diameter of fiber 19

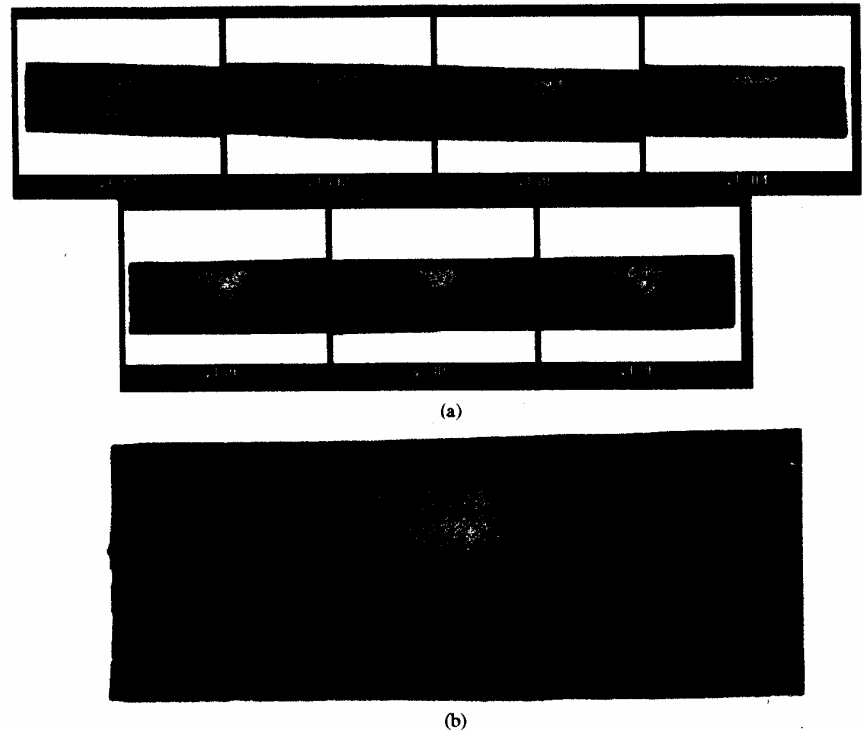


Fig. 6 Transmission images of fiber No. 19 using iron oxide tipped source rod. (a) the whole length of image (b) magnified image.

or the use of extra iron oxide in the molten zone may have been responsible.

3.3. Molten zone stability

Molten zones were typically unstable during YIG growth and pulsated along the growth direction. This instability may be related to (1) laser power, and therefore temperature fluctuations, (2) the incongruent melting behavior of these compounds, and/or (3) phase instability due to variations in or incorrect oxygen partial pressure.

Electron microprobe analysis (EPMA) revealed compositional fluctuations along the crystal axis. The fibers contained periodic inclusions of both yttrium orthoferrite ($YFeO_3$) and iron oxide. These inclusions may be due to an inappropriate temperature or melt composition at the growth interface arising from the unstable molten zones. The formation of the yttrium orthoferrite phase is a sign that the growth temperature occasionally exceeded the peritectic decomposition temperature (Fig. 1).

3.3.1. Influence of growth rate on composition and inclusions

At fast growth rates (20-60 mm/h), periodic inclusions formed along the entire length of the fiber. Fig. 7a shows a longitudinal cross section of fiber 4 grown in O₂ at 20 mm/h and Fig. 7b shows the axial compositional profile for Fe_2O_3 and Y_2O_3 . In this sample, the melt was frozen between the fiber and source rod, and the sample mounted, ground and polished along its length. This molten zone consisted of a multiphase solid made up of dendrite-structured $YFeO_3$ (light regions) and

Fe_2O_3 (dark regions). In this study fibers of uniform composition could only be obtained by using growth rates less than 12 mm/h and an air atmosphere. This is slower than that used for congruent materials grown by the LHPG method (3060 mm/h). Therefore, the growth rates in later experiments were kept in the range of 8-12 mm/h to reduce the formation of precipitates during the crystal growth.

Fig. 8 shows the composition profile of fiber 5 grown in air at 10-12 mm/h. A uniform stoichiometric YIG composition (within 0.5% error range) was obtained along the growth direction.

At these slow growth rates the secondary phases were significantly reduced. The slowest growth rate, 8 mm/h, seemed to give the best compositional homogeneity,

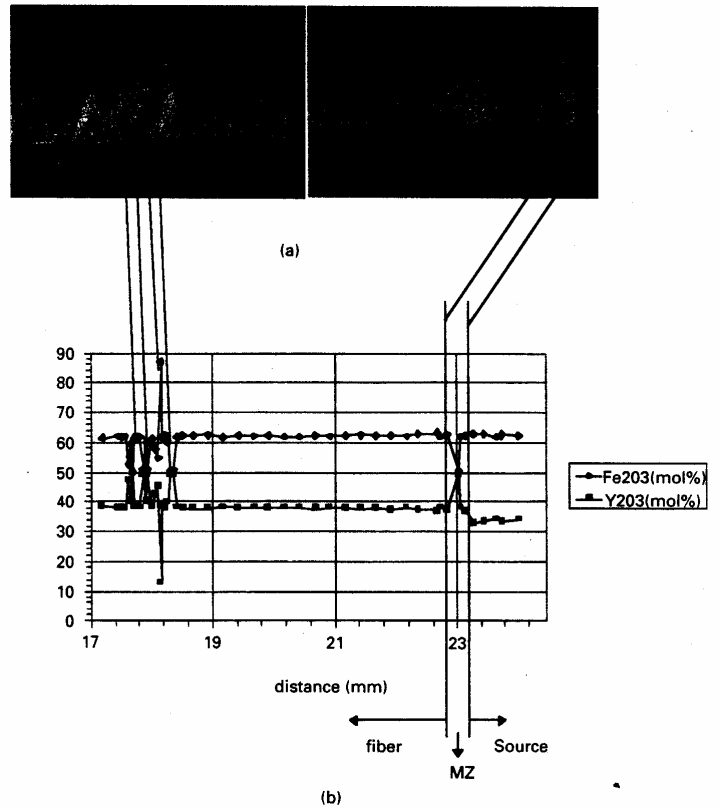


Fig. 7 Longitudinal cross section (a) and compositional profile (b) of fiber No. 4, where MZ stands for molten zone (growth rate: 20 mm/h)

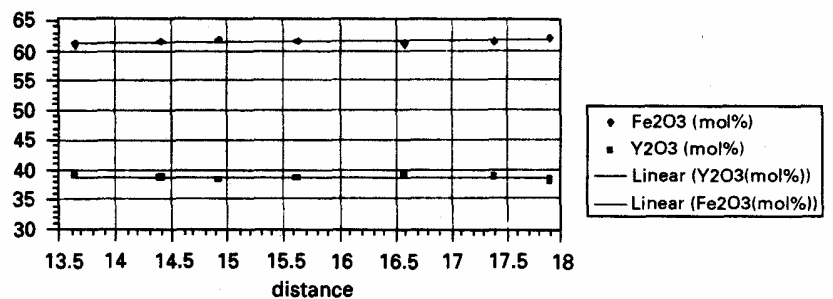


Fig. 8 Compositional profile of fiber No. 5 (growth rate: 10 mm/h)

which is not surprising for the growth of an incongruently melting material from solution. In solution growth, the solvent is rejected at the growth interface and nutrient material has to diffuse through the boundary layer to attach at the growth interface. If the growth rate is too fast then constitutional supercooling can take place and lead to second-phase incorporation. In the YIG system that would be the Fe_2O_3 phase.

The radial cross section of fiber 15 was also analyzed by EPMA. The compositional uniformity of this slow grown fiber (air atmosphere) is shown in Fig. 9. Small deviations within 2% from the ideal composition (less iron oxide and more yttrium oxide) were observed.

3.3.2. Laser power fluctuations

Perhaps the most important factor influencing molten zone stability in the LHPG method, and therefore fiber diameter uniformity and compositional homogeneity, is the variation of laser beam power with time. In the free running mode, the beam power of our laser varied between 15 and 19%. Even small power excursions can change the molten zone temperature and, thereby, its size. These fluctuations in zone length and perhaps shape can affect both the diameter of the crystal and its growth stability. The power fluctuations were reduced to less than 5% by introducing a feed back loop into the power control circuit. While the zone length fluctuations were significantly reduced in this manner, the diameter variations were only reduced slightly.

3.3.3. Effect of excess Fe_2O_3 in melt

The formation of YFeO_3 is expected (see the phase diagram in Fig. 1) if the temperature at the fiber-melt interface exceeds 1555°C in air due either to a reduced Fe_2O_3 concentration at the growth interface or laser power fluctuations. To keep the growth temperature below the peritectic point, and thereby prevent YFeO_3 formation, pure iron oxide was placed on the top of the source material to act as a solvent to lower the liquidus temperature. This was also expected to improve zone stability. Sample 19 was grown in this manner, and at a slow growth rate and air atmosphere. The molten zone, however, was still unstable. While the initial melting temperature dropped below 1600°C , fluctuations caused the molten zone temperature to go as high as 1640°C .

Another similar experiment for reducing the growth temperature to below the peritectic isotherm (fiber 21) involved using an iron oxide-rich source rod prepared by a standard ceramic processing technique (cold pressing and sintering). A small amount of this iron-rich source rod was placed on the tip of a stoichiometric YIG source rod and attached by laser melting. This was expected to drop the starting melting temperature below the peritectic, point B as shown in the phase diagram (Fig. 1), and hold it below that point during the growth. The result, however, was the same as for fiber 19 in which only pure iron oxide was used. It showed that the initial melting temperature dropped by up to 100°C and was therefore below the peritectic point. This condition did not continue for a long period. From the IR microscopic study of fiber No. 21, axial compositional variations due to iron oxide or orthoferrite precipitation were still observed in some areas of this fiber.

In growth experiment 21, the first 15 mm of fiber was grown in an air atmosphere and then the last portion (7 mm long) was grown in oxygen. The part grown in an oxygen atmosphere was crushed in an

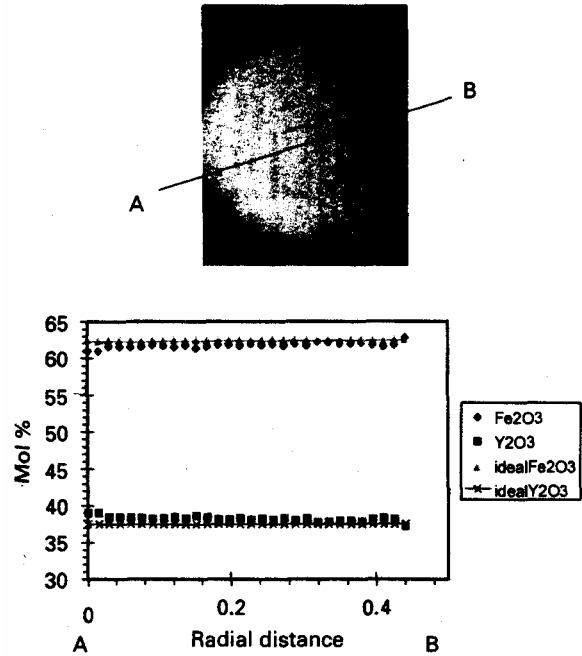


Fig. 9 Radial cross section and compositional profile of fiber No. 15

alumina mortar and pestle and the components analyzed by X-ray analysis. Small amounts of Fe_3O_4 were detected in the X-ray pattern. This iron oxide is thought to come from the surface material.

3.3.4. Meniscus angle of the molten zone

Stable oxide growth by the LHPG method is usually achieved at reduction ratios (d/D) in the range $1/2$ to $1/3$ [27]. Some YIG fibers (7-10 and 16) were grown with diameter reductions in excess of $1/3$. The diameter of these fibers was not constant. It was observed that stable molten zones were only obtained when the meniscus angle (θ in Fig. 3) was negative. The negative value reduces the allowable reduction to a maximum of $1/2$. It was found in these experiments, however, that the reduction must be greater than $1/2$ to maintain a uniform diameter in this material. Growing fibers with a negative angle made it very difficult to control fiber diameter for a long period of time. This was a result of an imbalance between the pulling and feeding rates.

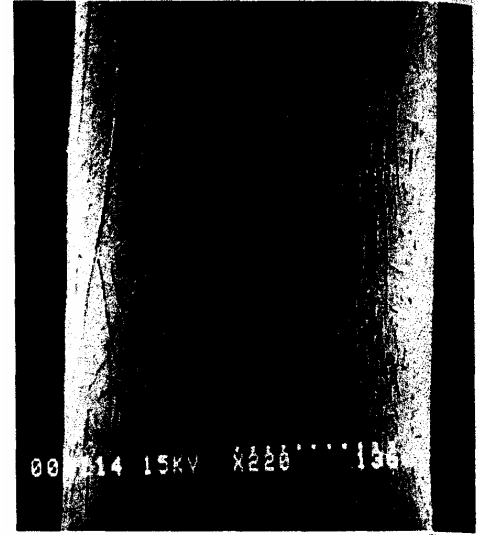


Fig. 10 SEM image of fiber No. 10 at 220x

3.4. Surface segregation

Higher magnification SEM images of all the fibers revealed surface ridges, as shown in Fig. 10. X-ray emission analysis of the ridges in the microprobe gave signals for iron and oxygen. A later fiber (15 in Table 1) was grown in the inverted position (with the fiber growing downward) to study whether these ridges might be due to iron oxides vaporized from the melt and condensing on the grown fiber. It was assumed that due to convection, the vaporized species would preferentially deposit on a cold surface above the melt rather than below it. Fiber 15 showed the same density of ridges as normal YIG and it appears that these features are associated with a growth phenomenon and not evaporation.

Fig. 11 shows the change of the surface morphology on fiber 15 due to changes in growth rates. As growth rate decreased, these ridges became discontinuous and finally transformed into islands. The radial cross sections of this fiber as a function of growth rate is also shown in Fig. 11. At fast growth rates (above 12 mm/h) the iron oxide ridges penetrated into the fiber and caused scattering of IR light transmitted through the fiber. However at slow growth rates (below 12 mm/h), ridge formation was significantly reduced.

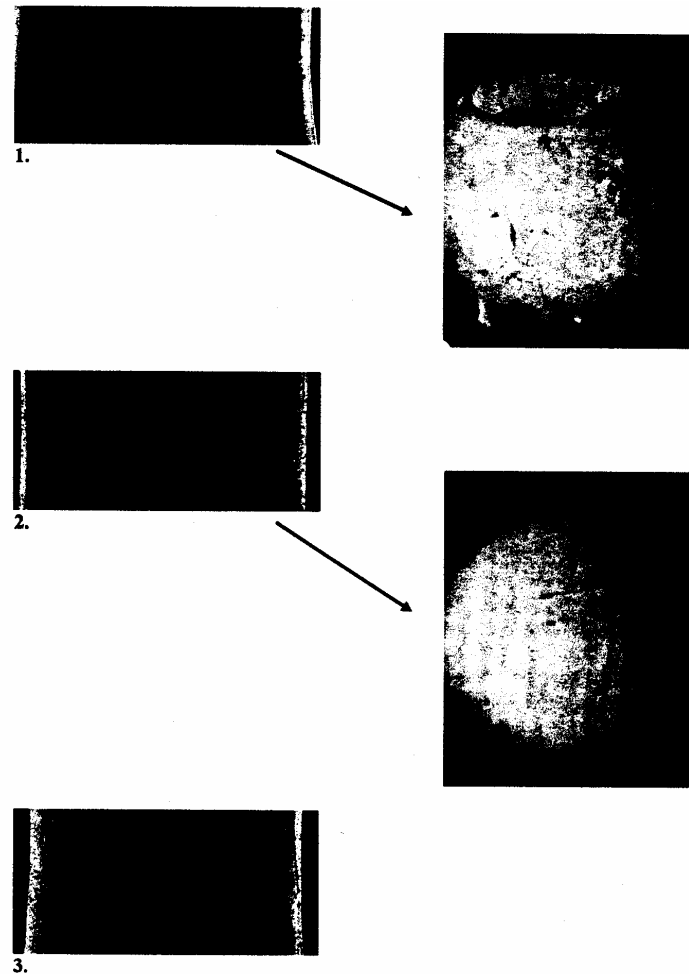


Fig. 11 Morphology change of fiber No. 15 according to the growth rates (growth rates: $1 > 2 > 3$)

The surface morphologies of YIG fibers grown in both air and oxygen were studied. Compared to those grown in oxygen, YIG fibers grown in air had very smooth surface morphologies, except for the iron oxide surface features. Rough, dimpled surfaces were observed on YIG fibers grown in oxygen. While YIG fibers grown in air were transparent, those grown in oxygen were opaque due to IR scattering from iron oxide inclusions. The melting temperature for YIG grown in oxygen (1620°C) is higher than that of fibers in air (1570°C).

3.5. Light scattering tomography

The three images of fiber 21 in Fig. 12 were produced by light scattering tomography (LST). The scattering, as observed by a microscope and CCD camera at 90° to the incident beam, was produced by defects in the fiber. The images are shown in grey scale that ranges from black for no scattering to white (at index fluid-fiber interface) for intense scattering. The fiber was immersed in the same index matching fluid used for optical microscopy and the index mismatch accounts for the large amount of surface scatter. The decrease in scattering intensity with increasing magnification was observed in these images as a color shift.

The 5 x image shows the entire length of the fiber. The images at 20 x are from the upper quarter area in the 5 x image. The two 20 x images were taken at different depths in the fiber. If the regions in the two 20 x images are examined, a variation of scattering intensity with depth is apparent. This is indicative of a distribution of scattering centers in the fiber that did not appear when the fiber was examined under an infrared microscope. The exact nature of these defects is not known at this time. The lower magnification images showed some evidence that the scattering centers may cluster into bands normal to the growth axis. This was not evident in the higher magnification images indicating they may be due to surface scatter.

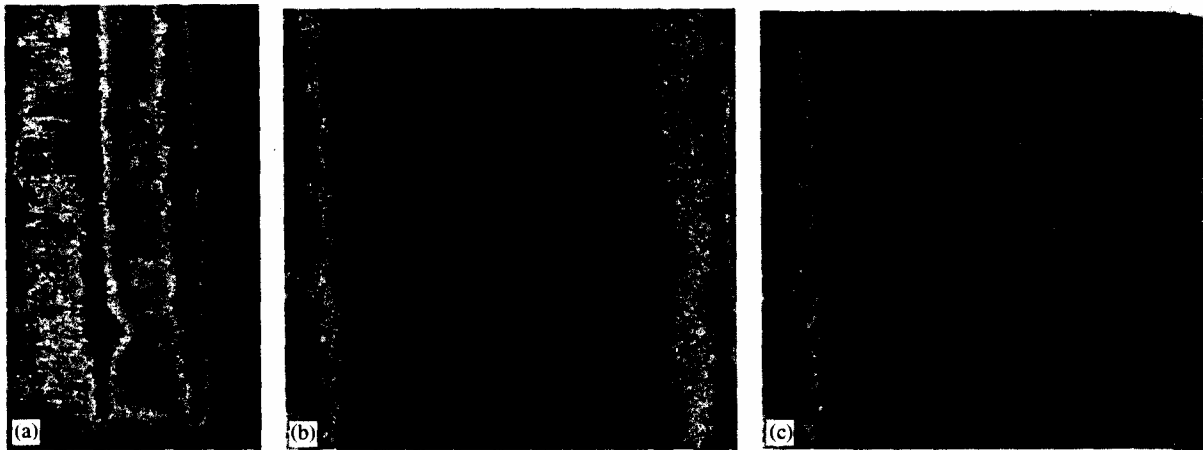


Fig. 12 Light scattering tomograph image of fiber No. 21 using a Nd-YAG laser. (a) 5 x, (b) 20 x, (c) 20 x, 100 deep into fiber.

3.6. Optical measurements

Transmittance along the fiber axis was measured by polishing the YIG endfaces, and illuminating one endface with 1.3 μm light. At the input face, the beam was apodized with centered pinholes. Light exiting the fiber was detected with a large area detector placed against the output facet. Transmittance T was obtained by dividing the power exiting the YIG (P_f) by that exiting the pinhole (P_p) ($T = P_f/P_p$).

For fiber 18, with a diameter of 125-150 μm over its 3.8 mm length, $T = 12.2\%$ for a 50 μm diameter

beam, and $T = 12.7\%$ for a $10\ \mu\text{m}$ beam. For these cases, losses can be attributed to both bulk and surface interactions since the beam diverges to the fiber diameter during propagation. For sample 19 (6.5 mm long, with diameter between 400 and $450\ \mu\text{m}$), $T = 20.0\%$ with a $50\ \mu\text{m}$ beam centered on the YIG diameter and $T = 15.4\%$ for a $100\ \mu\text{m}$ beam. For this larger diameter sample, the diverging beam would not reach the fiber diameter, so there could be less surface interaction in the absence of bulk scattering. Higher losses were observed when the probe beam entered the fiber off center, generally increasing with radius, indicating that surface scattering occurred. The role of iron valence state on optical loss has not yet been studied in these fibers.

4. Conclusions

Single crystal YIG fibers were grown by laser-heated pedestal growth method. The optimum growth rate for this incongruently melting material was below $10\ \text{mm/h}$. This is relatively low when compared with congruently melting materials processed by this method. The best seed-to-source rod reduction ratios (d/D) were in the range of $\frac{1}{2} - \frac{2}{3}$. Stable melting was obtained with a negative meniscus angle. Uniform fiber diameters were achieved only when the diameters were between 350 to $500\ \mu\text{m}$. Under these conditions, fibers grown in air had the best IR transparency. Optical losses along the fiber axis at $1.3\ \mu\text{m}$ appear to be largely caused by surface scattering.

Acknowledgements

This work was supported in part by the Department of Defense and the NSF-MRSEC Program through the Center for Materials Research at Stanford University. We specially thank Dr. R. Route at Applied Physics Department at Stanford for his help with using the LHPG apparatus.

References

- [1] F. Bertaut, F. Forrat, C.R. Acad. Sci. Paris 242 (1956) 382.
- [2] S. Geller, M.A. Gilleo, Acta Crystallogr. 10 (1957) 239.
- [3] W.P. Wolf, G.P. Rodrigue, J. Appl. Phys. 29 (1958) 105.
- [4] J. Nicolas, Microwave ferrites, in: E.P. Wohlfarth (Ed.), Ferromagnetic Materials, Vol. 1, North-Holland, Amsterdam, 1982, pp. 243-296.
- [5] J.F. Dillon Jr., J. de Phys. Radium 20 (1959) 374 and 379.
- [6] R.C. LeCraw, D.L. Wood, J.F. Dillon Jr., J.P. Remeika, Appl. Phys. Lett. 7 (1965) 27.
- [7] F.J. Kahn, P.S. Pershan, J.P. Remeika, Phys. Rev. 186 (1969) 891.
- [8] R. Young, T. Wu, I. Lin. Mat. Res. Bull. 22 (1987) 1475.
- [9] R. Young, T. Wu, I. Lin, J. Mat. Sci. 25 (1990) 3566.
- [10] A.H. Shaari, H.A.A. Sidek, M. Hashim, J. Mat. Sci. Lett. 12 (1993) 1838.
- [11] H.J. Van Hook, J. Amer. Ceramic Soc. 44 (1961) 208.
- [12] H.J. Van Hook, J. Amer. Ceramic Soc. 45 (1962) 162.
- [13] S. Nielsen, E.F. Dearborn, J. Phys. Chem Sol. 5 (1958) 202.
- [14] X.Z. Xu, W.Y. Jia, C.X. Liu, ACTA Physica Sinica 29 (1980) 1558.
- [15] S.H. Yuan, M. Pardavi-Horvath, P.E. Wiegen, J. Appl. Phys. 61 (1987) 3552.
- [16] G.A. Emelichenko, V.V. Masalova, G.F. Zakharyuguna, V.V. Petrov, Izvestiya Akad. Nauk SSSR, Neorg. Materialy 23 (1987) 837.
- [17] L.L. Abernethy, T.H. Ramsey Jr., J.W. Ross, J. Appl. Phys. 32 (1961) 1961.
- [18] I. Shindo, N. Kimizuka, S. Kimura, Mater. Res. Bull. 11 (1976) 637.
- [19] S. Kimura, I. Shindo, J. Crystal Growth 41 (1977) 192.
- [20] S. Kimura, K. Kitamura, I. Shindo, J. Crystal Growth 65 (1983) 543.

- [21] K. Hisatake, I. Matsubara, K. Maeda, T. Fujihara, N. Ichinose, I. Sasa, T. Nakano, *Phys. Status Solidi A* 104 (1987) 815.
- [22] W.G. Pfann, *Zone Melting*, 2nd ed., Wiley, New York, 1966.
- [23] R.S. Feigelson, *J. Crystal Growth* 79 (1986) 669.
- [24] Y. Furukawa, M. Fujiyoshi, F. Nitanda, M. Sato, S. Makio, *J. Crystal Growth* 143 (1994) 243.
- [25] Y. Suemune, H. Iwamura, M. Torii, U. Kihara, H. Goto, H. Yuri, *Proceedings of the International Conference on Ferrites*, 1980, p. 750.
- [26] D.L. Wood, J.P. Remeika, *J. Appl. Phys.* 37 (1966) 1232.
- [27] R.S. Feigelson, Growth of fiber crystals, in: E. Kaldis (Ed.), *Crystal Growth of Electronic Materials*, North-Holland, Amsterdam, 1985, p. 127.